Catalysis Today 394-396 (2022) 510–523

Contents lists available at ScienceDirect

Catalysis Today

journal homepage: www.elsevier.com/locate/cattod

Catalytic production of anilines by nitro-compounds hydrogenation over highly recyclable platinum nanoparticles supported on halloysite nanotubes

Cristian H. Campos [a], Krishnamoorthy Shanmugaraj [a,*], Tatiana M. Bustamante [a], Edgardo Leal-Villarroel [a], Victor Vinoth [b], Radhamanohar Aepuru [c], Ramalinga Viswanathan Mangalaraja [d,e], Cecilia C. Torres [f,*]

[a] Universidad de Concepción, Facultad de Ciencias Químicas, Departamento de Físico-Química, Edmundo Larenas 129, Casilla 160-C, Concepción, Chile
[b] Clean Technologies Laboratory, Faculty of Engineering, Universidad Católica de la Santísima Concepción, Concepción, Chile
[c] Departamento de Ingeniería Mecánica, Facultad de Ingeniería, Universidad Tecnológica Metropolitana, Santiago, Chile
[d] Advanced Ceramics and Nanotechnology Laboratory, Department of Materials Engineering, Universidad de Concepción, Concepción, Chile
[e] Technological Development Unit (UDT), University of Concepcion, Coronel Industrial Park, Coronel, Chile
[f] Departamento de Ciencias Químicas, Facultad de Ciencias Exactas, Universidad Andres Bello, Autopista Concepción-Talcahuano 7100, Talcahuano, Chile

ARTICLE INFO

Keywords:
Nitro compounds hydrogenation
Pt-based catalyst
Halloysite nanotubes
Recycling catalyst

ABSTRACT

Pt-nanoparticles supported on halloysite-nanotubes (HNTs) were selectively deposited onto the inner (Pt(IN)/HNT) or outer (Pt(OUT)/HNT) surface of the support to evaluate their operational stability on the cleaner and efficient hydrogenation of nitro compounds to produce their corresponding anilines. The formation of Pt^0-aggregates on the inner or outer surfaces was observed, with mean particles sizes of 2.4–2.9 nm. The catalysts were evaluated using ethanol as solvent and nitrobenzene as a model substrate at a temperature of 298 K, under 1 bar of H_2 pressure. The Pt(IN)/HNT catalyst showed better catalytic performance than Pt(OUT)/HNT, which was mainly attributed to the confinement effect of the Pt-nanoparticles inside the HNTs. However, the operational stability showed that Pt(OUT)/HNT retained its catalytic performance after 15 cycles, while the Pt(IN)/HNT catalyst suffered deactivation after the 5th cycle. The best catalytic system showed a moderate-to-high efficiency in the efficient hydrogenation of 7 nitro compounds used to produce their corresponding anilines, which are important pharmaceutical building blocks.

1. Introduction

The production of anilines from their corresponding nitro compounds has received substantial attention in recent years, as these substrates are used as building blocks for the synthesis of pharmaceuticals, dyes, pesticides, and other important fine chemicals [1–3]. Traditionally, the reduction of nitro compounds is achieved using reducing agents such as Fe, Zn, Sn, and sulfides, which generates large amounts of toxic residues, waste acids, and byproducts [4]. These processes are not environmentally sustainable due to the generation of harmful chemical wastes [5,6], which has promoted the development of alternate strategies. Specifically, the heterogeneous hydrogenation process is considered the best choice for the large-scale production of anilines from nitro compounds in industrial applications as the catalyst can be easily separated and reused [7–10]. Many heterogeneous catalysts have been reported using noble metals (Rh, Ru, Pd, Pt, Au, or Ag) as well as non-precious metal catalysts (Co, Ni, Cu, or Fe) supported on inorganic metal oxides for the direct hydrogenation of nitrobenzene to aniline [11–22]. Among them, Pt-mediated nitro compounds hydrogenation reactions are generally chemoselective for the corresponding aniline and use mild reaction conditions (i.e., temperatures below 353 K and H_2 pressures of 1–10 bar) [23–29]. High chemoselectivity for the conversion of nitro compounds to anilines has been obtained using Pt nanoparticles (NPs) supported on TiO_2 [23], zeolites [24], CeO_2 [26], Fe_2O_3 [27], or ZnO [28].

Despite the promising properties of Pt-supported catalysts, their efficient reuse remains challenging. To this end, several studies have reported heterogeneous catalysts based on Pt-NPs supported on carbon

* Corresponding authors.
E-mail addresses: shanmugaraj.chemist@gmail.com (K. Shanmugaraj), cecilia.torres@unab.cl (C.C. Torres).

https://doi.org/10.1016/j.cattod.2021.06.027
Received 29 January 2021; Received in revised form 12 May 2021; Accepted 25 June 2021
Available online 10 July 2021
0920-5861/© 2021 Elsevier B.V. All rights reserved.

carriers or surrounded by N-doped carbon materials, which control the activity, selectivity, and operational stability of the catalysts [29–32]. In addition, Shi et al. reported the use of 0.5 wt% ultrafine Pt-NPs supported on N-doped carbon nanotubes (CNTs) with oxygen functional groups as catalysts for the hydrogenation of nitrobenzene (NB), which showed stable catalytic performance over four continuous operation cycles using moderate reaction conditions (T = 298 K and H_2 pressure = 4.0 MPa) [30]. Li et al. reported the synthesis of Pt-NPs deposited on an ordered mesoporous carbon support (CMK-3) as an effective catalyst for the liquid-phase hydrogenation of NB [31]; the catalyst was recycled and reused at least fourteen times without any loss of activity or selectivity for the hydrogenation of NB in ethanol at 298 K and 4.0 MPa of H_2 pressure. Recently, an active and selective 1.89 wt% Pt/N-CMK-3 catalyst was developed for the hydrogenation of NB at 298 K and 2.0 MPa H_2 pressure, which showed excellent reusability (stable catalytic performance over at least eight continuous cycles) [29]. Despite their good performance, the synthesis and use of such carbon-based catalysts are not environmentally sustainable due to: (1) the production of toxic waste and high consumption of time and energy during catalyst synthesis; and (2) the selective hydrogenation reactions are carried out at harsh reactions conditions (high H_2 pressure and/or high temperature). As a result, the development of heterogeneous catalysts that have a lower environmental impact, e.g., can operate at mild conditions for the hydrogenation of nitro compounds is highly desirable and is currently attracting much interest in the field.

The use of metal NPs supported on nanotubes has emerged as a new strategy in heterogeneous catalysis and has been applied to organic synthesis [33–36]. Among them, halloysite nanotubes (HNTs; $Al_2Si_2O_5(OH)_4.nH_2O$) are considered an excellent nanocarrier for metal NPs [37–39]. This support is an aluminosilicate characterized by a hollow tubular structure, and has several unique advantages compared to other nanotube materials; it is abundant in nature, inexpensive, environment-friendly, inert, stable over a wide pH range (3–10), biocompatible, and thermally stable [38]. HNTs have an inner diameter of 10–20 nm and an external diameter of 40–60 nm, with tube length of 0.5–1.5 μm [38,40]. HNTs consist of aluminol (Al−OH) groups in the internal surfaces and siloxane/silanol (Si–O–Si/ Si-OH) groups on the external surface. Thus, the external surface is negatively charged and the internal surface is positively charged [38]. This difference in the inner/outer chemistry of the HNTs is unique among common support materials, where both surfaces of the HNTs can be easily modified with different materials to tailor the support for a wide range of applications [38–42]. In addition, the HNTs can provide an nanoscale void for immobilization of NPs in the inner nanotube surface, which can prevent aggregation of the NPs [38]. Therefore, the development of HNTs nanocomposites based on noble-metal NPs attached to the outer and inner surfaces has great potential for a wide range of applications [38, 41,43]. Recently, the confinement of Pd-NPs on HNTs was achieved and the composite material showed excellent results as a catalyst for the Suzuki–Miyaura cross-coupling reactions compared to other reported catalytic systems [44]. In addition, Ru/HNT nanocatalysts showed enhanced catalytic activity for the hydrogenation of phenols and olefins in water [45,46]. Other examples of the successful use of HNTs as catalytic supports include: HNT-supported Au and Ag nanoclusters for 4-nitrophenol (4-NP) reduction [37]; Pt@HNT catalysts for the reduction of potassium hexacyanoferrate(III) to potassium hexacyanoferrate (II) [47]; and Pt–Cu@HNTs used for 4-nitrophenol reduction with sodium borohydride ($NaBH_4$) [48]. In the field of heterogeneous hydrogenation, Pd@HNT-char nanocomposites were developed and used for catalytic hydrogenation of nitro compounds at mild reaction conditions (298 K and 1 bar H_2 pressure) reaching moderate catalytic performance after eight catalytic cycles [49]. These results encourage the use of HNT as a benign support for developing highly active, selective, and recyclable catalysts for the efficient reduction of NB and other substituted nitro compounds.

The aim of this study was to develop catalysts suitable for environmentally friendly liquid-phase hydrogenation of nitroarenes of pharmaceutical interest at mild reaction conditions. Herein, we report the design, preparation, characterization, and catalytic evaluation of novel HNT-supported Pt-NPs catalysts. The Pt-NPs were prepared using a simple reduction process using $NaBH_4$ as the reducing agent. The design of the catalyst involved the selective deposition of Pt-NPs on the pre-activated inner surface of HNT (Pt(IN)/HNT) or the aminosilane-assisted deposition of Pt-NPs on the HNT outer surface (Pt(OUT)/HNT) to evaluate the effect of the catalytic site. The catalysts were evaluated for the selective reduction of NB as a representative test compound under mild reaction conditions (298 K and 0.1 MPa H_2 pressure) using ethanol as the solvent. Recycling experiments were performed using the best catalytic system under optimized operational conditions. Our findings are expected to promote the use of HNT-supported catalysts for the reduction of nitro compounds of pharmaceutical interest, which are valuable building blocks for the chemical industry.

2. Experimental

2.1. Materials

Nitrobenzene, K_2PtCl_6, $NaBH_4$, absolute ethanol, (3-aminopropyl) trimethoxysilane (APTMS), and sodium hydroxide (NaOH) were purchased in Merck. 2-Chloro-5-nitrobenzotrifluoride and HNTs were procured from Sigma-Aldrich. 4-(4-Nitrophenyl)morpholin-3-one, 4-(2-fluoro-4-nitrophenyl)morpholine, 2-(diethylamino)ethyl-4-nitrobenzoate, 2-chloro-1-((3-fluorobenzyl)oxy)-4-nitrobenzene, and 1-(4-chlorophenoxy)-2-nitrobenzene were synthesized and characterized according to our previous reports [50–53]. Hydrogen and nitrogen gases used for the hydrogenation reactions were of ultrahigh purity (>99%).

2.2. Synthesis of the catalysts

2.2.1. Synthesis of 1 wt% Pt(IN)HNT

The HNTs were first activated using a reported protocol [48]. HNTs (1.0 g) were dispersed into 100 mL of distilled water under sonication for 10 min. The solution was adjusted to pH 10 with NaOH and stirred for 12 h. Then, the suspension was centrifuged at 6000 rpm for 10 min, washed several times with water, and dried in a hot air oven prior to use as pre-treated HNTs. To prepare Pt(IN)/HNT with Pt-NPs deposited on the inner surface of the pre-treated HNTs, 0.1 g of pre-treated HNTs were dispersed in 50 mL of distilled water and sonicated for 10 min. Then, an appropriate volume of K_2PtCl_6 (9.6 mmol·L^{-1}) and NaOH (1.0 mmol·L^{-1}) solutions were added and stirred for 4 h. Subsequently, 10 mL of a freshly prepared aqueous $NaBH_4$ (50 mmol·L^{-1}) solution was added and the solution was stirred for another 1 h to completely reduce the Pt precursor. The resulting solution was centrifuged and thoroughly washed with water. Finally, the product was dried at 323 K for 12 h.

2.2.2. Synthesis of 1 wt% Pt(OUT)/HNT

The HNTs were modified with APTMS using a previous reported protocol [54]. First, 5.0 g of HNTs were ultrasonically dispersed in 100 mL of toluene and 0.5 mL of APTMS solution was added, followed by heated at 383 K for 12 h. Then, the amine-functionalized HNT support were finally collected by centrifugation and washed with acetone: toluene (3:1) mixture and dried at 323 K for 12 h to produce NH_2-HNTs. Then, 0.3 g of NH_2-HNTs was dispersed in 150 mL of distilled water and sonicated for 10 min. Subsequently, an appropriate volume of K_2PtCl_6 (9.6 mmol·L^{-1}) was added and stirred for 4 h. Then, 10 mL of a freshly prepared $NaBH_4$ solution (50 mmol·L^{-1}) was added and the mixture was stirred for 1 h. Finally, the solid was collected and thoroughly washed with water, and then dried at 323 K for 12 h to produce Pt(OUT)/HNT.

2.3. Characterization

FT-IR (Thermo Scientific, USA) in the range of 4000–500 cm^{-1} equipped with a Attenuated Total Reflectance (ATR) accessory with a germanium crystal which has a penetration depth of approximately 0.65 μm [55]. The spectra were collected in the range of 4000–400 cm^{-1} with sixteen cans at 4 cm^{-1} resolution. Observed area was 250 μm^2 with a pixel size of 6.25 μm × 6.25 μm. The pixel size corresponds to the size covered by each detector element of a linear array detector of pure mercury–cadmium–telluride (MCT) arranged as 16 gold-wired infrared detector elements. The background spectrum was collected before analyses of each sample. Hyperspectral images and IR spectra were operated using Spectrum Image software (PerkinElmer Inc.). Thermogravimetric (TG) studies were conducted using a Mettler Toledo Thermogravimetric TGA/SDTA 851 using an O_2 flow of 5 mL min^{-1} and a heating rate of 5° min^{-1} from 298 to 1273 K. Dismissing the adsorbed water in pristine-HNT, the mass loss decrease allows the determination of the grafting quantity (μmol g^{-1}) of the functionalized carriers by the following equation:

$$grafting = \frac{\frac{m_{NH_2-HNT}}{(100-m_{NH_2-HNT})} - \frac{m_{HNT}}{(100-m_{HNT})}}{M_{APTMS}} \quad (1)$$

Where $m_{NH2\text{-}HNT}$ is the mass loss percentage of the APTMS modified supports on HNT, m_{HNT} is the mass loss corresponding to the amount of the physiosorbed water in the HNT (corresponding to the mass loss between 25 and 150 °C, and M_{APTMS} is the molar mass of the APTMS.

The elemental metal content was quantitatively determined for selected fresh catalysts using inductively coupled plasma mass spectrometry (ICP-MS) using a Perkin Elmer ICP-MS instrument after microwave-assisted digestion of the samples in a nitric/hydrochloric acid solution. Transmission electron microscopy (TEM) images were obtained using a JEOL JEM-1200 EX II microscope. Assuming a population of monodispersed (i.e., with the same size) metal particles, the dispersion, D (%), is related to the mean particle size by a simple formula:

$$D(\%) = \frac{1.01}{d_{TEM}(nm)} \times 100 \quad (2)$$

where D corresponds to the ratio of the number of surface metal atoms to the total number of metal atoms [27].

Powder X-ray diffraction (XRD) patterns were recorded using a Rigaku diffractometer Rad-II-C (Rigaku, Tokyo, Japan) with Ni-filtered Cu $K_{\alpha 1}$ ($\lambda = 1.5418$ Å) radiation, in the 2Θ range 20°–90°. The specific surface area and pore size distribution were obtained using the Brunauer-Emmett-Teller (BET) method, and the pore-size distributions were estimated using the BJH method based on N_2 adsorption desorption isotherms recorded at 77 K using a Micromeritics ASAP 2010 apparatus. The surface composition of the materials was analyzed by X-Ray photoelectron spectroscopy (XPS) using a Surface Analysis Station 1 electron spectrometer (XPS RQ300/2, Staib Instrumente GmbH, Langenbach, Germany) equipped with a hemispherical electron analyzer DESA 150 detector/2700 V and non-monochromatic Al-Kα (1486.6 eV) X-ray source. The spectra were fitted with a Gaussian–Lorentzian function with variable ratios. The C 1s core-level of adventitious carbon at a binding energy (BE) of 284.8 eV was used as an internal standard.

2.4. Hydrogenation of nitro compounds

The catalytic hydrogenation of nitro compounds was performed in a semi-batch Parr type reactor using 20 mg of catalyst and a substrate weight suitable to attain $mole_{substrate}/mole_{Pt} = 5000$ based on the metal content determined by ICP analysis. The reaction was carried out at 0.1 MPa H_2 pressure with 50 mL absolute ethanol and mechanical agitation up to 700 rpm at the desired temperature. Prior to the reaction, the reactor was flushed three times with a N_2/H_2 gas mixture and pressurized with the desired pressure of H_2 gas. The conversion and selectivity of the reaction was identified by gas chromatography (GC; Hewlett Packard HP 4890 D) equipped with an HP-5 capillary column and a flame-ionization detector.

The conversion ($X_{\text{nitro compound}}$) and selectivity ($S_{\text{product}}$) toward the product were calculated using the following equations.

$$X_{\text{nitro compound}}\% = \frac{[\text{nitro compound}]_i - [\text{nitro compound}]_t}{[\text{nitro } compound]_i} \times 100 \quad (3)$$

$$S_{\text{product}}\% = \frac{[product]_t}{[\text{nitro compound}]_i - [\text{nitro compound}]_t} \times 100 \quad (4)$$

where de $[\text{nitro compound}]_i$ correspond to the initial nitroarene concentration and $[\text{nitro } compound]_t$ is the nitroarene concentration at the corresponding time.

The turnover frequency (TOF) value for the catalytic hydrogenation reaction was calculated as follows for 10% conversion of nitroaromatics.

$$\text{TOF}\left(\text{min}^{-1}\right) = \frac{mol\ of\ substrate\ hydrogenated}{mol\ of\ metallic\ Pt\ surface\ (time\ min)} \quad (5)$$

the mol of metallic Pt surface were estimated from the total metal loading from the ICP analysis and normalized by the metallic dispersion measured by TEM approximation (Eq. (1)).

The catalyst recycling experiments were performed following our previous procedure [50]. The catalysts were collected after each cycle by centrifugation and washed three times in absolute ethanol. After each run, the supernatant was collected and analyzed using ICP-MS to estimate the amount of Pt-NPs leaching. Then, the solid was collected and dried in a static air oven at 323 K overnight. The hydrogenation of the nitro compound to produce anilines was performed at the optimal operational conditions determined from the NB reaction. The conversion and selectivity of these reactions were identified by GC-MS (Perkin Elmer GCMS-SQ8T).

3. Results and discussion

3.1. Characterization of NH_2-HNT support

The silanization of HNTs with APTMS can be achieved by direct condensation of hydrolyzed silanes groups with Si-OH or Al-OH surface hydroxyls (grafting reaction); in our case, the surface was modified to achieve the selective deposition of Pt-NPs on the outer surface of the HNTs [47]. Yuan et al. have reported that selective immobilization of trialcoxy-propylamine silanes on the inner/outer surface of the HNT followed an oligomerization/condensation pathway which depends on water physically adsorbed on the surface of nanotube [56]. In the presence of pristine support (hydrated HNT), the APTMS hydrolyze thoroughly, and considerably these molecules are grafted onto the outer surface of the HNT by oligomerization process. To quantify the grafting percentage, Fig. 1A displays the TG mass changes for both HNT and NH_2-HNT materials. For the HNTs, a mass loss of 2.4% in the 298–433 K range was observed, which corresponds to the removal of the interlayer and surface-adsorbed H_2O of the sample. A second mass loss of 8.9% in the range of 650–850 K was attributed to the dehydroxylation of the HNT support [57]. After the APTMS immobilization treatment, NH_2-HNT showed three mass losses in the ranges of: (1) 298–450 K, attributed to the loss of H_2O physisorbed as well as the solvent and/or APTMS molecules remaining from the immobilization process on the support; (2) 500–650 K, attributed to the covalently bonded APTMS; and (3) 663–860 K, attributed to the removal of Al-OH groups and decomposition of covalently bonded APTMS in a multistep process [57, 58]. These results showed a total mass loss for this material of 4.3%, corresponding to a surface grafting of 0.24 $mmol_{NH2}g^{-1}$.

Fig. 1B shows ATR-FTIR characterization of pristine-HNTs and

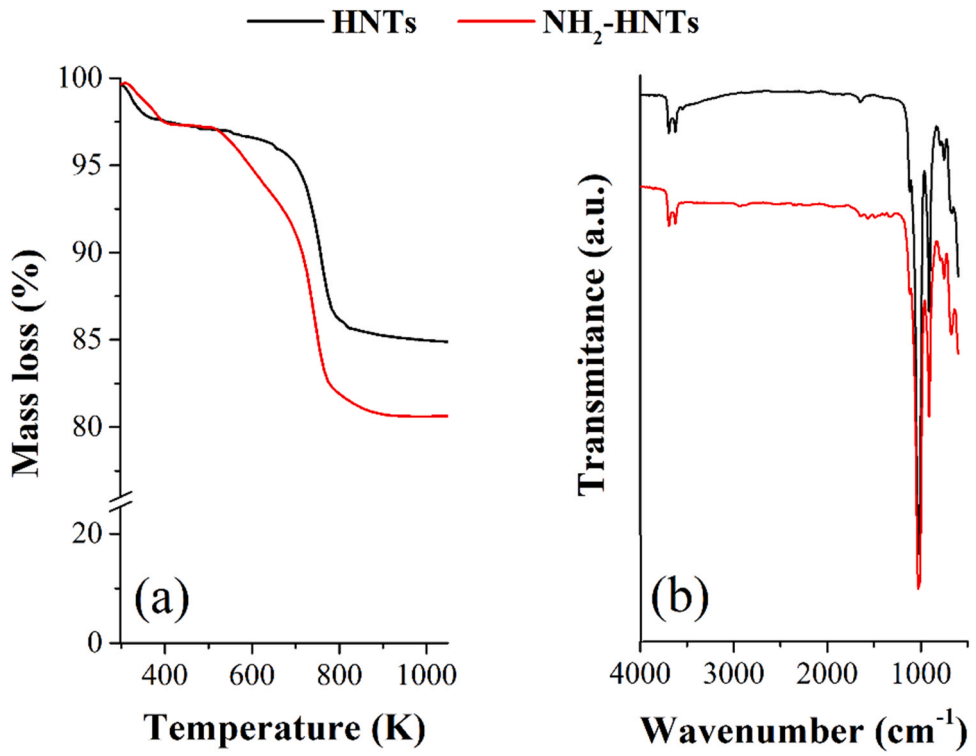
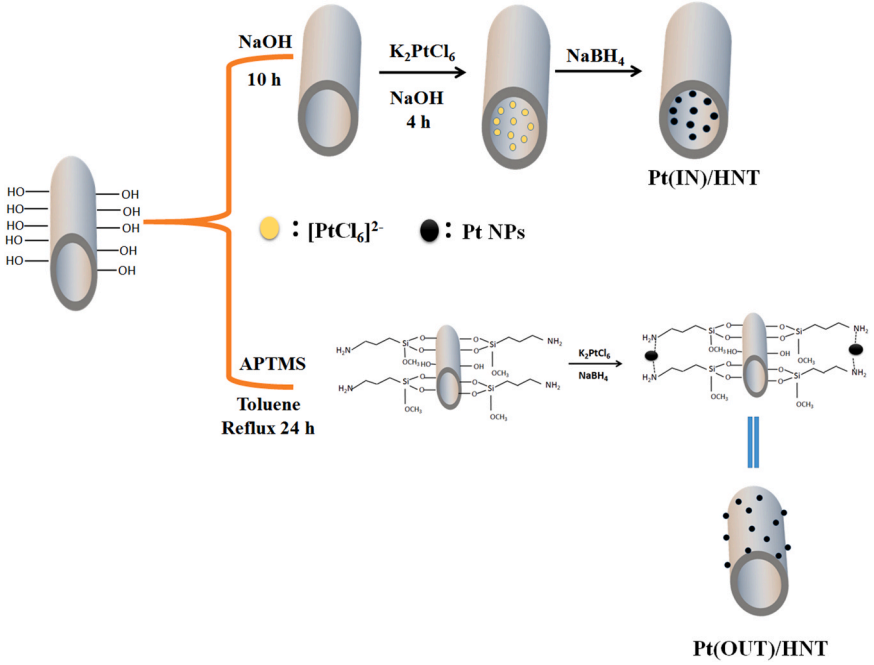


Fig. 1. Thermal and spectroscopic of HNTs and NH_2-HNT supports. (a) TG-O_2 analysis between room temperature and 1273 K and (b) ATR-FTIR spectra in the range of 500–4000 cm^{-1}.

APTMS-functionalized support. The pristine-HNTs displays bands at 3693 and 3621 cm^{-1} attributed the stretching vibration of the -OH groups present at the inner surface of the HNTs [57]. The deformation of O-H stretching of intercalated water was found at 1632 cm^{-1}. Furthermore, the NH_2-HNT solid showed bands attributed to the C–H stretching vibrations of -CH_2 groups at 2958, 2925, and 2868 cm^{-1}, while the band at 1534 cm^{-1} is ascribed to bending vibrations of the N-H from the -NH_2 group. The inner surface -OH groups are not modified by the APTMS immobilization onto HNTs. This result suggest that the APTMS was preferably immobilized on the outer surface of the tube, which in line with the previous reported results [56].

3.2. *Characterization of the catalysts*

The preparation of both Pt(IN)/HNT and Pt(OUT)/HNT is schematically illustrated in Scheme 1. For the synthesis of Pt(IN)/HNT, a small



Scheme 1. Schematic of the synthesis of Pt(IN)HNT and Pt(OUT)HNT catalysts.

quantity of NaOH was added to the mixture containing the Pt precursor and HNTs to adjust the pH to 10. Subsequently, $NaBH_4$ was introduced to complete the Pt^{4+} reduction. The addition of NaOH is crucial to promote the adsorption of the metal precursor on the inner surface of the HNTs [48]. The negatively charged $[PtCl_6]^{2-}$ ions can undergo two simultaneous processes at basic pH in the core of the HNTs: (1) $[PtCl_6]^{2-}$ may transform into $[PtCl_{4-x}(OH)_x]^{2-}$ [59]; and (2) all negative ions can be strongly anchored onto the inner surface by ligand exchange with Al-OH/Al-O$^-$. As a result, the Pt-NPs were deposited inside the HNTs after the reduction process. In the case of Pt(OUT)/HNT, APTMS was used as a coupling agent to modify the outer HNT surface with NH_2 groups [47,56]. The Pt-NPs synthesis method was designed to enhance metal precursor deposition by chemical adsorption on the outer surface, assisted by the presence of $–NH_2$ functional groups. The metal precursor and the NH_2-HNTs carriers were reacted in ethanol to promote the ligand exchange of the $[PtCl_6]^{2-}$ ion to produce $[PtCl_{4-x}(NH_2\text{-HNTs})_x]^{2-}$ species during the first 4 h of the reaction. Considering the TG results, we propose that the $–NH_2$/Pt mole ratio was ~5, which indicates optimal ligand exchange during the synthesis of the catalyst. Then, the $NaBH_4$ aqueous solution resulted in the reduction of Pt^{4+} to Pt^0, while the increase of the pH to 10 promoted the chemical stabilization of Pt-NPs by the $–NH_2$ surface groups (APTMS pKa = 9.8 [60]).

To confirm the metal loading in the catalysts, ICP-MS characterization was performed, where the results are shown in Table 1. The similarity of experimental and nominal metal contents indicated the absence of appreciable metal loss during synthesis and confirmed the chemical composition of the as-prepared catalysts.

The morphologies of Pt-NPs loaded on the inner/outer surfaces of the HNTs were investigated using TEM, as shown in Fig. 2. For Pt(IN)/HNT, all of the observed Pt-NPs were spherical and homogeneously distributed. The Pt-NPs with an average diameter of 2.90 ± 0.4 nm were highly localized in the core of the HNTs (Fig. 3a) with 35% estimated metal dispersion as resumed in Table 1. In the case of Pt(OUT)/HNT, the Pt-NPs were homogeneously distributed on the outer surface of the HNTs with a particle size of 2.43 ± 0.3 nm (Fig. 3b), which is in line with a 42% of Pt dispersion calculated by TEM characterization (Table 1).

XRD analysis was performed to analyze the crystal structure of the as-prepared catalysts (Fig. 3). The HNT sample showed characteristic diffraction peaks at 2Θ = 12.0°, 20.0°, 24.7°, 36.0°, 38.5°, 54.8°, and 62.5°, which corresponded well with JCPDS No. 29-1487 [49]. There were no significant peaks observed for Pt species for either the Pt (IN)/HNT or Pt(OUT)/HNT catalyst, attributed to the excellent dispersion, low loading, and nanoscale size of Pt-NPs present in both samples [61].

Fig. 4 shows the N_2 adsorption-desorption isotherms for pre-treated HNT, NH_2-HNT, Pt(IN)HNT, and Pt(OUT)HNT materials. The corresponding data for the pristine HNT sample is shown in the Supplementary material (Fig. S1). All of the isotherms had a shape corresponding to type-IV isotherms with an H3 hysteresis loop, indicating the presence of mesoporous and cylindrical pores [62,63]. The BET surface areas (S_{BET}) and average pore widths are listed in Table 1. The surface areas of both the pre-treated and pristine HNT samples were similar, indicating that the pores of the HNTs were not blocked or corroded after the NaOH treatment. The S_{BET} and pore diameter of Pt(IN)/HNT were smaller than those of the pre-treated HNT sample, which was attributed to the selective Pt-NPs deposition on the inner surface of the HNTs [62]. In the case of NH_2-HNT, the S_{BET} and pore diameter were very similar to those of the pristine-HNT sample, confirming that the APTMS linker was deposited preferentially on the outer surface of the support. A previous study [56] showed that the use of a pristine-HNT support during APTMS immobilization treatment promoted the anchorage of the linker on the outer surface by the presence of air in the HNT core that prevented the penetration of APTMS. Indeed, in the case of Pt(OUT)/HNT, after the surface coverage with Pt-NPs, the catalyst had textural properties very similar to those of NH_2-HNT. This result is consistent with the TEM characterization, which confirmed the preferential deposition of the Pt-NPs on the outer surface of the NH_2-HNT support.

Table 1
Physicochemical properties of the synthesized catalysts.

Sample	Pt_{ICP} (wt%)[a]	Pt d_{TEM} (nm)	D_{TEM} (%)	S_{BET} (m^2 g^{-1})	d_{pore} (nm)[b]	V_{pore} (cm^3 STP)
Pristine-HNT	–	–	–	53	13.9	0.26
Pre-HNT	–	–	–	45	13.7	0.21
Pt(IN)/HNT	0.91 (1.0)	2.90 ± 0.4	0.35	38	12.3	0.12
NH_2-HNT	–	–	–	36	13.1	0.19
Pt(OUT)/HNT	0.98 (1.0)	2.43 ± 0.3	0.42	38	12.9	0.15

[a] Nominal values in brackets.
[b] Calculated using the BHJ method and the adsorption branch.

The surface chemistry of both catalysts was characterized using XPS (Fig. 5). The presence of the Pt $4d_{5/2}$ peak at a BE = 314.8–315.0 eV in both samples indicated the presence of Pt^0. Therefore, the treatment with $NaBH_4$ facilitated the complete reduction of the metal precursor, in agreement with results reported previously [64]. Table 2 shows the atomic ratios of the catalyst components on the surface of Pt/Al catalysts, as analyzed by XPS. The Pt/Al atomic ratio for Pt(IN)/HNT was lower than that measured for Pt(OUT)/HNT, which indicates the preferential deposition of Pt on the outer surface.

3.3. Catalytic performance

The catalytic hydrogenation of NB in the liquid phase was used as a benchmark reaction to evaluate the catalytic performance of both Pt (IN)/HNT and Pt(OUT)/HNT catalysts. To confirm the catalytic activity of our proposed catalysts, control experiments were also performed using: (a) the supports (pristine HNT, Pre-HNT, and NH_2-HNT supports); (b) the catalysts in the absence of H_2 (replaced by N_2); and (3) the reaction in the absence of the catalysts, which showed negligible catalytic activity (see Table S1). We observed that the HNTs act only as an inert support during NB hydrogenation, where the catalytic reduction of the substrate by the hydrogen transfer reaction (with ethanol acting as a hydrogen donor) was discharged during the reaction performance.

Fig. 6a shows the conversion curves as a function of time for the NB consumption in the presence of both catalysts, where pseudo-first kinetics was observed. This trend indicates that the Pt-NPs deposited in the inner/outer surface acted as the active sites for the hydrogenation of NB. The catalytic activity of Pt(IN)/HNT was better than that of Pt(OUT)/HNT. For Pt(IN)/HNT, 100% conversion of NB was achieved at 180 min with k = 0.87 ± 0.04 $min^{-1}{\cdot}g_{cat}^{-1}$, whereas Pt(OUT)/HNT reached 100% conversion after 300 min of reaction with k = 0.43 ± 0.03 $min^{-1}{\cdot}g_{cat}^{-1}$. In addition, Pt(IN)/HNT and Pt(OUT)/HNT reached 100% and 99.2% of selectivity towards aniline at 5 h and 7 h of reaction, respectively (Fig. 6b).

The heterogeneous hydrogenation of NB is a complex multistage process, which involves two possible routes, as illustrated in Scheme 2. The first reaction pathway corresponds to the direct route (red) that involves the consecutive formation of nitrosobenzene and N-phenylhydroxylamine intermediaries to give aniline (AN) as the final product. The second pathway is the condensation route (blue) that corresponds to the recombination of the nitrosobenzene and N-(phenyl)-hydroxylamine intermediates to form azoxybenzene, azobenzene, and/or hydrazobenzene as products [65]. In our case, in the initial reaction stage, nitrosobenzene was observed as the intermediate with moderate selectivity (Fig. S2). At low conversions of nitrobenzene (~10%), the only products observed in the reaction profiles for both catalysts were nitrosobenzene and AN. No coupling products were observed at this conversion, suggesting that the hydrogenation of nitrobenzene is

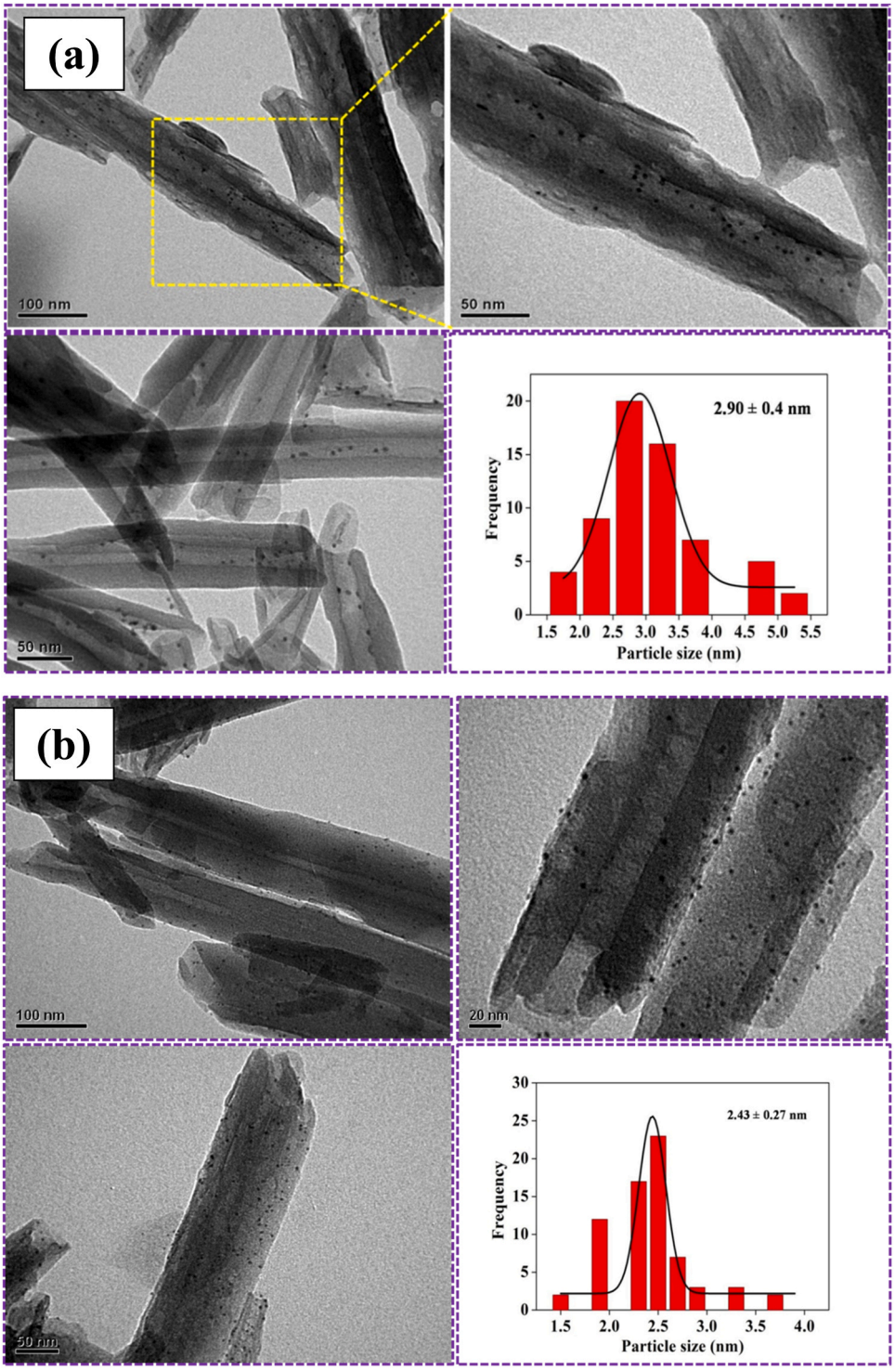


Fig. 2. TEM micrographs and particle size distribution of (a) Pt(IN)/HNT and (b) Pt(OUT)/HNT catalysts.

mediated through the direct route as the main reaction pathway [6,66]. When the reactions proceed further, the concentration of nitrosobenzene significantly decreased and finally AN was observed as the sole reaction product. In our case, the two catalysts showed different reaction rates and product distributions for NB hydrogenation (see Fig. 6a-b), which suggests that the hydrogenation of NB was dependent on the location of the Pt-NPs on the HNT surface. The enhanced catalytic activity of Pt(IN)/HNT was attributed to the confinement of the Pt-NPs within the HNTs. In the lumen of the HNTs, the adsorption of the NB molecules was restricted within the limited free space, which favored the interaction between the active phase, the chemisorbed hydrogen, and the substrate to produce the desired product. However, in the case of Pt(OUT)/HNT, the hydrogenation rate may have been lower due to the competition of NB adsorption on the inner/outer surface. These results suggest that the confinement provided by the HNT lumens improved the hydrogenation capacity by the increase of the NB concentration around the Pt-NPs.

Table 3 presents the results of recent studies of the catalytic performances of various heterogeneous monometallic supported Pt catalysts for the hydrogenation of NB [27,30,31,67–72]. The optimal catalysts

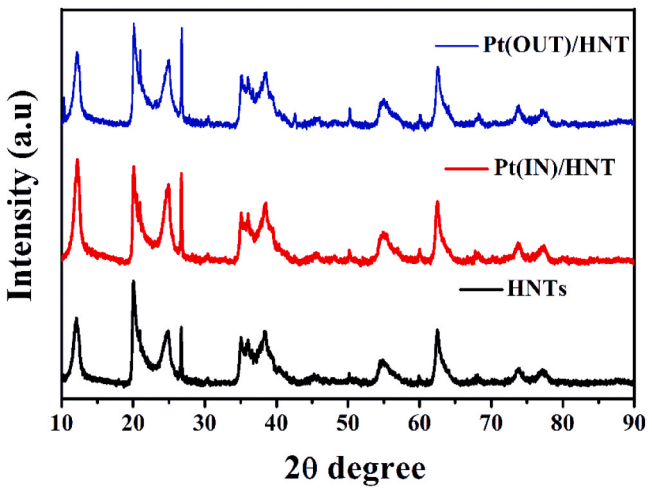


Fig. 3. XRD patterns of pristine HNTs and the two different catalysts.

were based on carbon supports (entries 3, 5–8), where higher TOF values than those obtained for our catalysts were reported. Among them, Pt/RGO-EG (entry 7) showed the highest catalytic performance reaching a TOF of 1138 min^{-1}. However, in all these examples, the reaction conditions used for the hydrogenation of NB included higher H_2 pressure and/or higher reaction temperature than used in our study. In the case of our catalysts, both systems showed excellent catalytic performance at 7 h of reaction, where the TOF values were higher than those reported for the catalytic systems operating at similar reaction conditions (entries 1 and 9). Is important to note that the Pt/Fe_2O_3 (entry 1) and Pt/H-NCNTs (entry 2) catalysts had TOF values similar to those of our catalysts, but their reaction design included the use of harmful solvents, such as toluene or ethylbenzene.

The effects of temperature on the catalytic hydrogenation of NB over Pt(IN)/HNT and Pt(OUT)/HNT are shown in Fig. S3. When the temperature increased from 285 to 323 K, the time required to complete the reduction of NB was shorter for both catalysts as a result of the higher rate of the reaction at higher temperature. Interestingly, even at the lower temperature of 285 K, both catalysts exhibited maximum conversion level at different reaction time. The performance of both catalysts was successfully fit using a pseudo-first-order relationship (Fig. S4), where the pseudo-first-order constant (k) was estimated at different temperatures from the slope of the linear plot. Furthermore, the activation energy (E_{aa}) for the hydrogenation of NB over our catalytic systems was determined using the Arrhenius equation shown below.

$$ln \quad k = \ln \quad A - \frac{E_{aa}}{R} \bullet \frac{1}{T} \tag{6}$$

Here, A is the frequency factor and T is the reaction temperature (K). The plot of ln k vs 1/T can be derived as shown in Fig. 7. The E_{aa} for hydrogenation of NB over Pt(IN)/HNT and Pt(OUT)/HNT are calculated to be 25.2 and 27.4 kJ mol^{-1}, respectively.

The low E_{aa} values obtained for both catalysts were consistent with

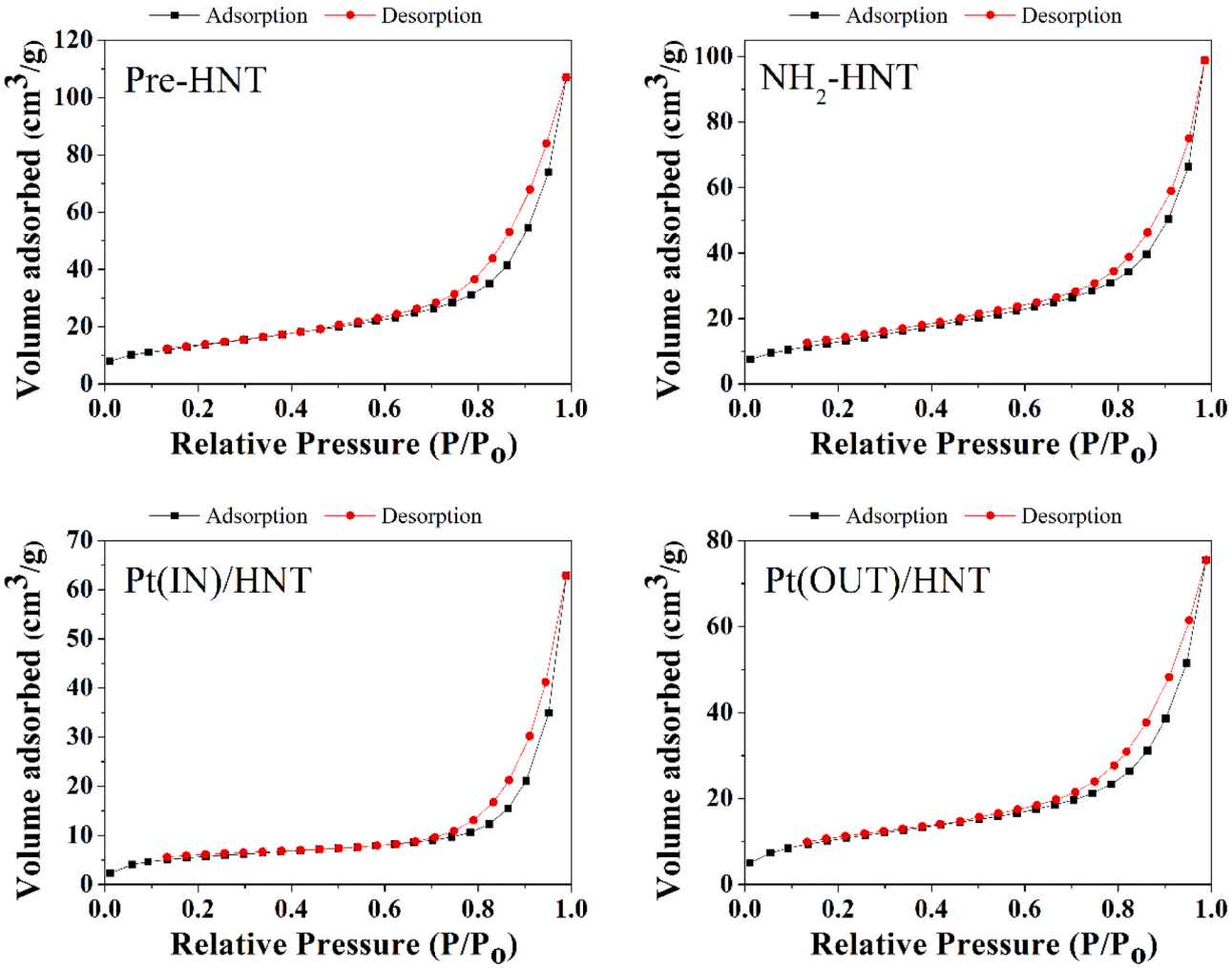


Fig. 4. N_2 adsorption–desorption isotherms of the prepared materials at 77 K.

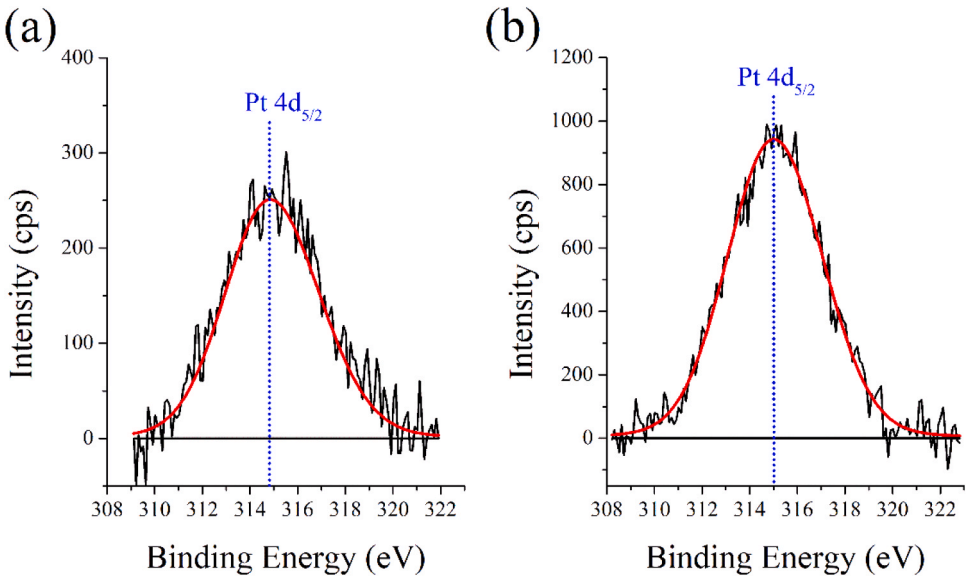


Fig. 5. XPS spectra of Pt $4d_{5/2}$ for the as-synthesized (a) Pt(IN)/HNT and (b) Pt(OUT)/HNT catalysts.

Table 2
Binding energies (eV) of the internal electrons and atomic surface ratio of the as-synthetized catalysts.

Sample	Al 2p (eV)	Si 2p (eV)	Pt $4d_{5/2}$ (eV)	Pt/Al at	Pt/Si at
Pt(IN)/HNT	74.5	103.2	314.8	0.41	1.08
Pt(OUT)/HNT	74.6	103.4	315.0	3.46	0.17

their superior NB hydrogenation ability compared with the earlier reported metal-based catalysts (Table 4) [65,73–75]. The catalysts in entries 3–5 all showed higher E_{aa} values than our catalytic systems. Nevertheless, in the catalysts based on Pd-NPs supported on CNTs or N-doped CNTs (NCNTs) (entries 1 and 2) E_{aa} values similar to those of our catalysts were observed. Among them, Pd/CNT showed the lowest $E_{aa} = 20.0$ kJ mol^{-1}, which was attributed to the unique balance between the size of the Pd-NPs and the metal–support interaction between the Pd and CNTs [65]. However, it is generally accepted that Pt is the preferred metal for hydrogenation, whereas Pd-based catalysts are non-selective catalysts for the hydrogenation of halo-nitro compounds [51]. In this context, our Pt-based nanocatalysts show promise as a versatile catalytic system for the environmentally friendly hydrogenation of multifunctional nitro compounds.

3.4. Recyclability

Catalyst recycling and recovery experiments are important for analyzing the environmental and economic aspects of these materials in both industrial and academic research applications. To investigate the stability and reusability of the as-synthesized Pt(IN)/HNT and Pt(OUT)/HNT catalysts, a series of recycling experiments for the catalytic hydrogenation of NB were performed under the same reaction conditions with similar conversion and selectivity values for both catalysts. The reusability of Pt(IN)/HNT and Pt(OUT)/HNT for hydrogenation of NB was analyzed by observing the changes in the conversion and selectivity over consecutive runs, as depicted in Fig. 8a-b. For Pt(IN)/HNT, the catalytic activity (100% conversion) and selectivity (100%) towards AN were almost unchanged after 5 h of reaction for up to five reaction cycles. After the sixth cycle, 100% conversion and selectivity was achieved

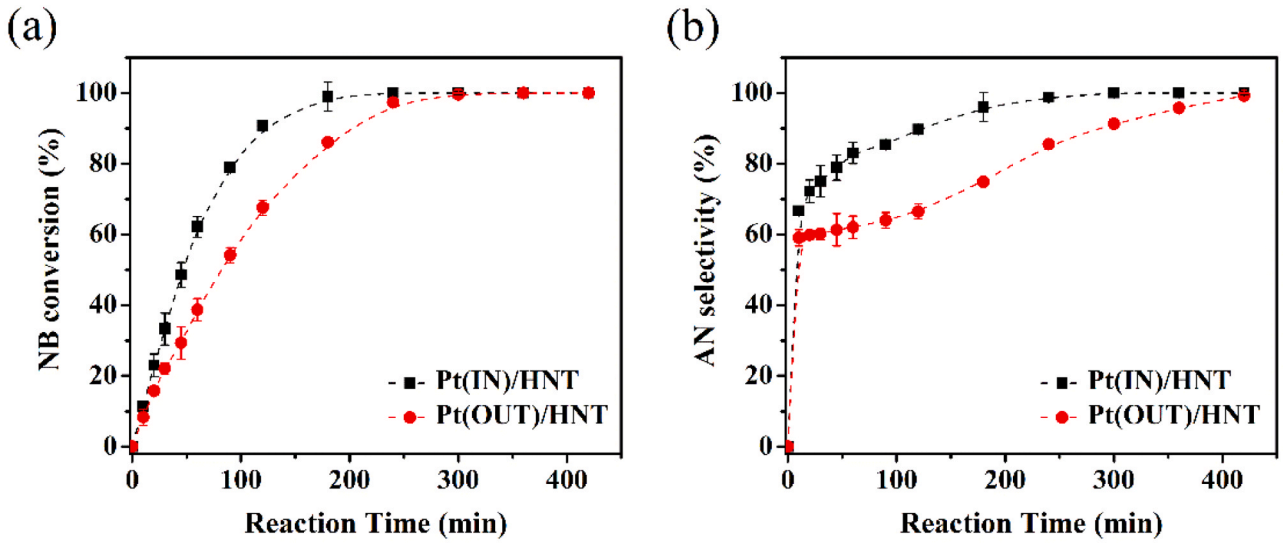
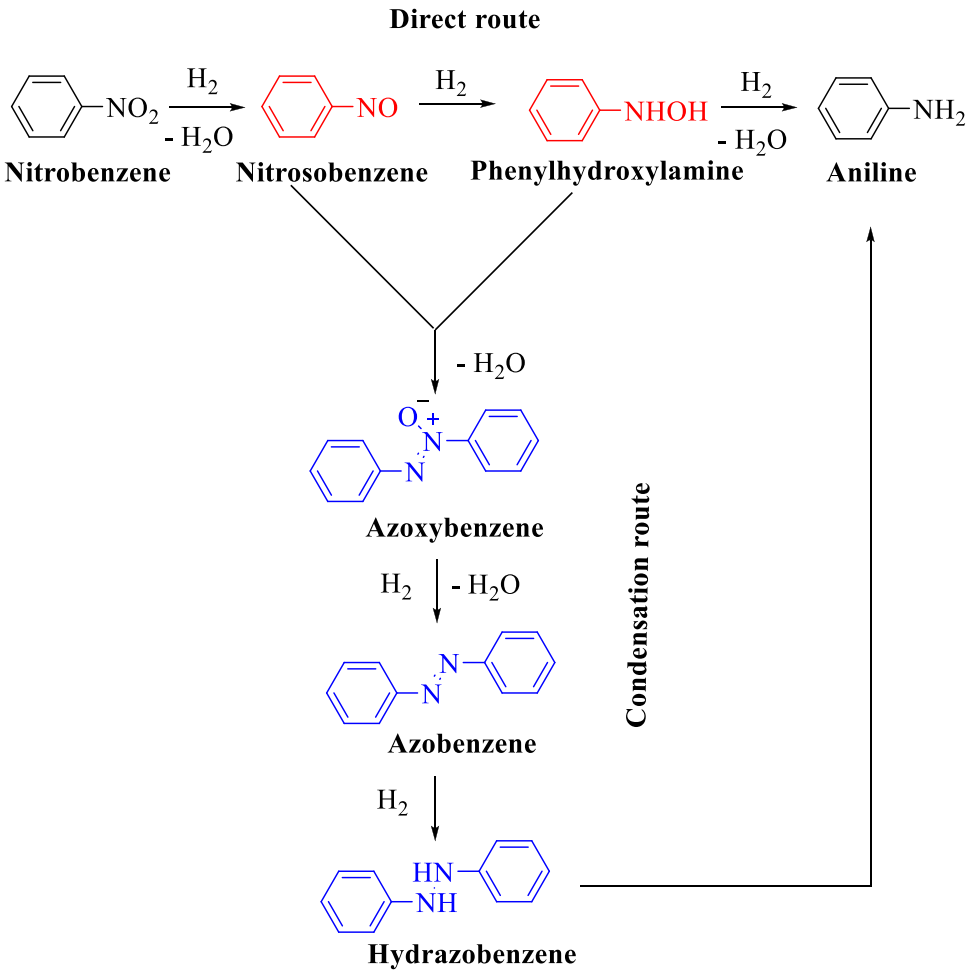


Fig. 6. (a) NB conversion and (b) AN selectivity as a function of reaction time for hydrogenation of NB over Pt(IN)/HNT and Pt(OUT)/HNT catalysts. Mass catalysts 0.020 g at 298 K, with 0.1 MPa of H_2, 50 mL of ethanol, and a stirring speed of 700 rpm.



Scheme 2. Reaction pathways for nitrobenzene hydrogenation. (For interpretation of the references to colour in this figure legend, the reader is referred to the web version of this article.)
adapted from [65].

Table 3
Comparison of the catalytic activities of heterogeneous Pt-based catalysts for NB hydrogenation.

Entry	Catalyst	Time (min)	Pt loading (wt %)	Catalyst mass (mg)	Solvent	H_2 pressure (MPa)	T (K)	X_{NB} (%)	S_{AN} (%)	TOF (min^{-1})	Ref
1	Pt/Fe_2O_3	120	0.2	50	toluene	0.5	303	96	99	130	[27]
2	Pt/H-NCNTs	120	0.5	10	ethylbenzene	0.5	313	98	99	190	[30]
3	Pt/CMK-3	10	5.0	50	water–ethanol	4.0	298	98	99	660	[31]
4	SAC-Pt/C	50	0.3	40	ethanol	0.1	313	99	97	2.0	[67]
5	Pt/N-CMK-3	90	1.9	40	ethanol	2.0	313	99.9	99	314	[68]
6	Pt/MWNT	7	5.0	5.0	Solvent free	4.0	333	100	100	1115	[69]
7	Pt/RGO-EG	20	1.3	75	ethanol	1.0	293	100	89	1138	[70]
8	Pt/TiO_2/RGO	8	2.1	12	Solvent free	4.0	333	100	100	980	[71]
9	Pt/AlO(OH)	150	2.6	100	methanol–water	0.1	303	83	78	60	[72]
10	Pt(IN)/HNT	300	1.0	20	ethanol	0.1	298	100	100	259	This work
11	Pt(OUT)/HNT	420	1.0	20	ethanol	0.1	298	100	98	118	This work

after 6 h of reaction. In the case of the seventh cycle, 79% conversion was obtained after 7 h of reaction, while 100% selectivity was achieved, but it required a much longer reaction time (24 h). The hydrogenation process could be completed by extending the reaction time for the Pt (IN)/HNT catalyst after the fifth cycle. Furthermore, ICP measurements were performed to evaluate Pt leaching into the supernatant after each catalytic cycle. The accumulative Pt loss from Pt(IN)/HNT after six continuous catalytic cycles times was 34.7% compared to the initial Pt content. Similarly, TEM characterization of the reused Pt(IN)/HNT catalyst indicated a slight aggregation of Pt-NPs with an increase of particle size from 2.9 nm to 6.1 nm (Fig. 8c). Hence, the Pt(IN)/HNT catalyst suffered deactivation as a result of the combined effect of metal leaching and Pt-NPs sintering. The increase in the size of the Pt-NPs decreased the number of exposed Pt atoms, and hence, number of active sites available in the hydrogenation process.

In the case of Pt(OUT)/HNT, after 15 cycles, the catalyst maintained

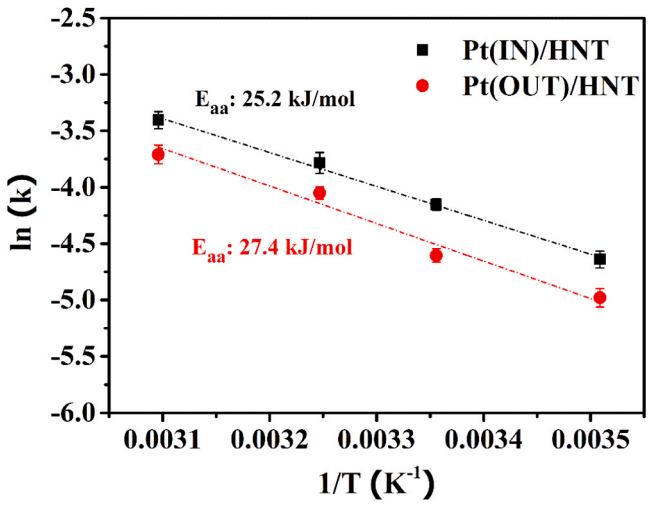


Fig. 7. Apparent activation energies (E_{aa}) calculated for hydrogenation of NB over Pt(IN)HNT and Pt(OUT)HNT. Reaction conditions: mass catalysts 0.020 g, 0.1 MPa H_2 pressure, 285–323 K, 50 mL of ethanol, and stirring speed of 700 rpm.

Table 4
Comparison of the E_{aa} values of various catalysts for the hydrogenation of NB.

Entry	Catalyst	Solvent	H_2 Pressure (MPa)	E_{aa} (kJ mol^{-1})	Ref
1	Pd/NCNTs	Ethanol	0.5	28.1	[65]
2	Pd/CNTs	Ethanol	0.5	20.0	[65]
3	Co@NMC-800	Ethanol	1.0	35.9	[73]
4	Pd/C	Methanol	3.0	35.1	[74]
5	Ag-OMS-2	2-Propanol	2.5	44.3	[75]
6	Pt(IN)/HNT	Ethanol	0.1	25.2	This work
7	Pt(OUT)/HNT	Ethanol	0.1	27.4	This work

its high catalytic activity without any loss in conversion or selectivity. ICP analysis of the recycled Pt(OUT)/HNT catalyst confirmed that the Pt loading remained unchanged after 15 cycles, while the supernatant did not contain Pt, even after the last catalytic cycle. In addition, TEM analysis of Pt(OUT)/HNT used for 15 cycles showed no change in the particle size of the Pt-NPs, which indicates that the Pt(OUT)/HNT catalyst had good stability under the optimal reaction conditions (Fig. 8d). The catalytic stability of Pt(OUT)/HNT was double that of Pt (IN)/HNT (7 cycles). This superior catalytic stability is attributed to the strong attachment of the Pt-NPs on the outer surface of the HNTs provided by the immobilized APTMS, which prevented metal leaching, as well as the undesired aggregation of the Pt-NPs. Despite the enhanced catalytic activity of the Pt(IN)/HNT catalyst, the use of the inner surface of the HNTs as a capping agent for Pt-NPs stabilization inside the HNTs did not prevent Ostwald ripening after consecutive catalytic cycles. These data clearly highlight the critical role of APTMS in controlling the operational stability of HNT-supported Pt-NPs for the efficient and environmentally friendly catalytic hydrogenation of nitro compounds.

3.5. *Chemoselective hydrogenation of pharmaceutical nitro compounds*

Owing to the excellent recyclability and good catalytic activity of the Pt(OUT)/HNT catalyst, it was further evaluated for the hydrogenation of multifunctional nitro compounds, which are relevant building blocks for the synthesis of pharmaceutical compounds. The operational conditions for nitro compounds hydrogenation were identical to those used for the reduction of NB. Table 5 shows the conversion and selectivity for the corresponding amines, indicating that all of the substrates were successfully reduced at different reaction times. In the case of the nitro compounds used to produce the anilines used to synthesize the anticancer drug Sorafenib (entry 1) [76], antibiotic medicine Linezolid [50] (entry 2), and anticoagulant drug Rivoraxaban (entry 3) [50], the maximum conversion and selectivity (nitroso-intermediary <1%) to their corresponding anilines was observed at shorter reaction times than for the NB substrate. The improved hydrogenation performance for 2-chloro-5-nitrobenzotrifluoride (entry 1) was attributed to the combined effect of the strong electron-withdrawing properties of the –Cl atom at the *para* position and $–CF_3$ functional group at the *meta* position with respect to the $–NO_2$ moiety. Indeed, a similar behavior was observed for 4-(2-fluoro-4-nitrophenyl)-morpholine (entry 2) which has a –F atom at the *meta* position. Hence, it is expected that these withdrawing substituents are favorable for increasing the hydrogenation rate as this reaction occurs via a transition state with a developing negative charge [66]. In the case of 4-(4-nitrophenyl)morpholin-3-one (entry 3), the carbonyl group also withdraws electrons from the benzene ring as it engages in effective π-delocalization with the morpholine N lone pair, thus reducing the electron donating properties of the substituent compared to NB.

The hydrogenation of 2-chloro-1-((3-fluorobenzyl)oxy)-4-nitrobenzene (entry 4) is used to produce their corresponding aniline used as a building block for the synthesis of the drug Lapatinib [53]. Despite the electron-withdrawing nature of the –Cl atom in the *meta* position, the presence of 3-fluoro-benzyloxy group in the *para* position compensates this effect through its higher electron-donating ability. Furthermore, Pt (OUT)HNT showed a different catalytic profile for the hydrogenation of 2-(diethylamino)ethyl-4-nitrobenzoate (entry 5), which is used for the preparation of the procaine anesthetic drug [52]. The hydrogenation reaction at the operational conditions used for NB reduction showed the maximum nitro compounds conversion, while the production of the desired amino-arene only reached 5% selectivity. In the reaction media, ethyl 4-nitrobenzoate (60%) and ethyl 4-aminobenzoate (35%) were detected as byproducts. This behavior was attributed to the combined effect of the solid-acid sites of the HNT support and the electronic structure of the 2-(diethylamino)ethyl-4-nitrobenzoate. Despite the external surface modification of the HNTs with APTMS to produce the Pt (OUT)/HNT catalyst, the carrier had solid-acid sites (Brønsted and Lewis acid sites), which are excellent catalytic sites for the esterification of fatty acid by aliphatic alcohols [77]. In addition, the $–NO_2$ group in the *para* position with respect to the ester moiety could promote the electrophilic behavior of this carbonyl group, which enhances the support-catalyzed trans-esterification reaction to produce the ethyl 4-nitrobenzoate product. We propose that the production of ethyl 4-aminobenzoate is a consequence of the hydrogenation of the ethyl 4-nitrobenzoate byproduct. To avoid the formation of these byproducts and confirm our hypothesis, the hydrogenation of 2-(diethylamino)ethyl-4-nitrobenzoate was performed using ethyl acetate as solvent. In this scenario, 2-(diethylamino)ethyl 4-aminobenzoate was detected as the main reaction product, reaching 76% selectivity after 7 h of reaction, and 84% selectivity after 24 h of reaction. In addition, 4-nitrobenzoic acid and 4-aminobenzoic acid where detected as the only reaction byproducts. This could be due to the 2-(diethylamino)ethyl-4--nitrobenzoate hydrolysis catalyzed by the solid-acid sites of the HNT carrier producing H_2O as a result of the reduction of $–NO_2$ to $–NH_2$ during the hydrogenation process [52].

The substrates 1-nitro-2-phenoxybenzene (entry 6) and 1-(4-chlorophenoxy)-2-nitrobenzene (entry 7) [53] were used as intermediaries to produce their corresponding amino-arenes, which are used to synthesize Nimesulide (an anti-inflammatory drug) [78] and Loxapine (for schizophrenia treatment) [53], respectively. Both substrates showed high selectivity to the desired product, while the conversion reached 25% for 1-nitro-2-phenoxybenzene and 58% for 1-(4-chlorophenoxy)-2-nitrobenzene after 24 h of reaction. These results are consistent

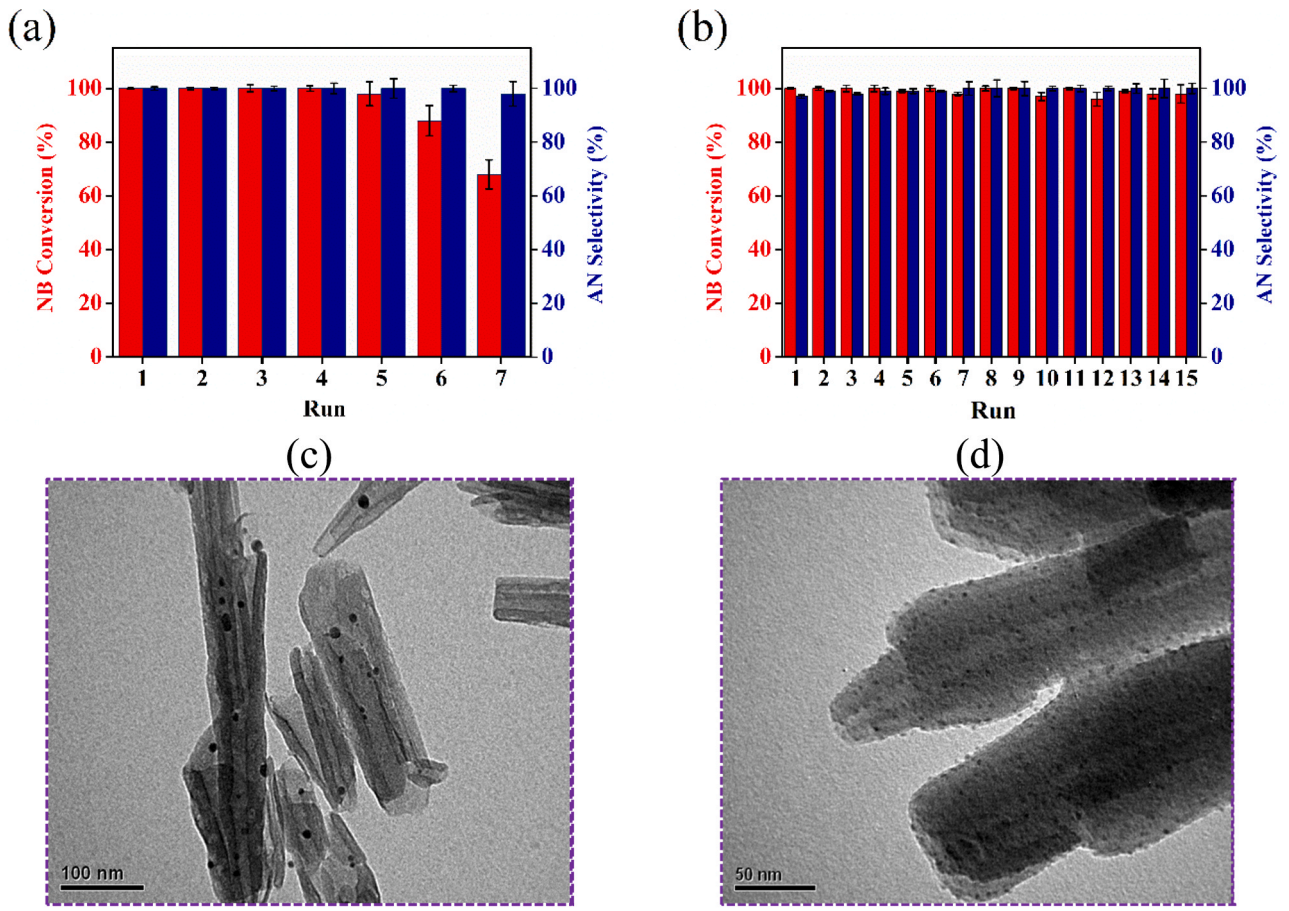


Fig. 8. Recyclability of (a) Pt(IN)HNT and (b) Pt(OUT)HNT catalysts for NB hydrogenation. Post-reaction TEM characterization of (c) Pt(IN)HNT and (d) Pt(OUT)HNT. Reaction conditions: mass catalysts 0.020 g, 0.1 MPa H_2 pressure, 298 K, 50 mL of ethanol, and stirring speed of 700 rpm. The reaction was stopped at 180 min for Pt(IN)/HNT system and at 420 min for the Pt(OUT)/HNT catalyst.

with the presence of the phenoxy group in the *meta* position with respect to the $–NO_2$ moiety. This substituent group can affect the hydrogenation rate by its electron-donating properties. However, in the case of 1-(4-chlorophenoxy)-2-nitrobenzene, the –Cl atom in the *para* position provided an inductive effect to the phenoxy group, increasing the hydrogenation ability compared with the 1-nitro-2-phenoxybenzene molecule. The hydrogenation capacity of the Pt(OUT)/HNT catalyst was also evaluated at 333 K for the molecule shown in entry 6, which showed an increased activity reaching 58% conversion and 100% selectivity to 3-phenoxyaniline after 24 h of reaction.

All the examples listed in Table 5 demonstrate the versatility and excellent catalytic performance of the Pt(OUT)/HNT catalyst for chemoselective $–NO_2$ hydrogenation to provide the desired $–NH_2$ group, even in the presence of other reducible and/or reactive functionalities operating under environmentally friendly conditions.

4. Conclusion

This work reports the efficient, versatile, and environmentally sustainable cleaner hydrogenation of nitrobenzene and nitro compounds of pharmaceutical relevance using recoverable and recyclable HNT-supported Pt-NPs catalysts. Two different methods were used to preferentially deposit Pt-NPs on the inner or outer surface of the HNTs, where homogeneous distribution of Pt^0 NPs with similar sizes were achieved. Both Pt(IN)/HNT and Pt(OUT)/HNT catalysts were active in the reduction of nitrobenzene at mild reaction conditions, with a maximum conversion and selectivity above 99%, and TOF of the best catalyst reaching 205 min^{-1}. These results indicate a significant improvement compared with previously reported Pt-based catalysts operating at the same reaction conditions. Catalyst recycling experiments showed that the Pt(OUT)/HNT system was the most stable, as it did not suffer from Pt leaching and sintering. The Pt(OUT)/HNT catalyst was active in the hydrogenation of 7 nitro compounds with electron withdrawing and/or donating substituents. Our results demonstrate that the Pt(OUT)/HNT catalyst has great promise as highly recyclable and stable catalysts for the cleaner hydrogenation of nitro compounds of pharmaceutical interest under mild reaction conditions, with minimal environmental impact.

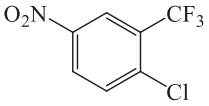
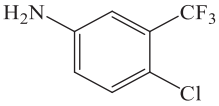
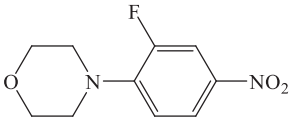
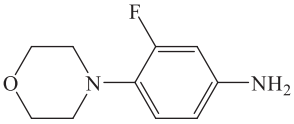
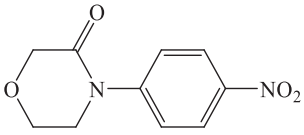
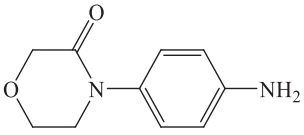
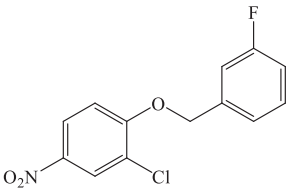
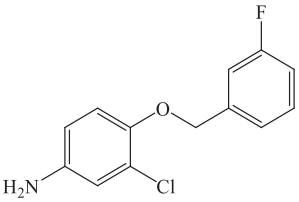
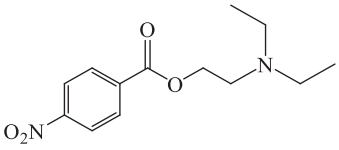
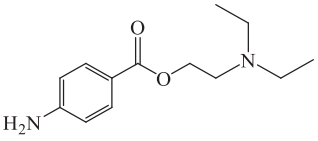
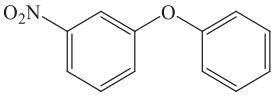
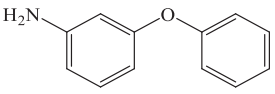
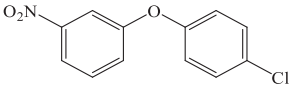
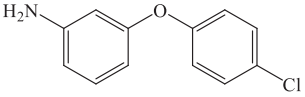
Funding

This work was supported by CONICYT-ANID FONDECYT postdoctoral grant 3180232 and FONDECYT grant 1191465.

CRediT authorship contribution statement

Krishnamoorthy Shanmugaraj: Data curation, Investigation, Methodology, Project administration, Writing – original draft, Resources. **Tatiana M. Bustamante:** Conceptualization, Data curation. **Edgardo Leal-Villarroel:** Data curation. **Victor Vinoth:** Data curation. **Radhamanohar Aepuru:** Formal analysis, Software. **Ramalinga Viswanathan Mangalaraja:** Investigation. **Cecilia C. Torres:** Supervision, Methodology, Resources. **Cristian H. Campos:** Formal analysis, Writing – review & editing.

Table 5
Catalytic hydrogenation of large pharmaceutical nitro compounds to their corresponding amines over Pt(OUT)/HNT.

Entry	Substrate	Product[a]	Time (h)	X_{nitro} (%)	$S_{aniline}$ (%)
1			3	> 99	99.3
2			5	> 99	100
3			6	> 99	99.4
4			8	> 99	99.6
5			3 7[c] 24[c]	100 88 99	5.0[b] 76.6[d] 84.5[d]
7			24 24[e]	25 58	100 100
6			24	60	100

[a]Reaction Conditions: 0.020 mg Pt(OUT)/HNT catalyst, 0.1 MPa H_2 pressure, 298 K, 50 mL ethanol, and stirring speed of 700 rpm.
[b]Reaction byproducts: ethyl 4-nitrobenzoate (60%) and ethyl 4-aminobenzoate (35%).
[c]Reaction solvent: ethyl acetate.
[d]Reaction byproducts: 4-nitrobenzoic acid and 4-aminobenzoic acid.
[e]Reaction temperature: 333 K

Declaration of Competing Interest

The authors declare that they have no known competing financial interests or personal relationships that could have appeared to influence the work reported in this paper.

Acknowledgements

The authors acknowledge the Unidad de Equipamiento Científico - MAINI, Universidad Católica del Norte for the XPS analysis (CONICYT-Programa FONDEQUIP XPS EQM140044 2014–2016). C.C. Torres

thanks CONICYT, PAI/Concurso Nacional Inserción de Capital Humano Avanzado en la Academia Convocatoria, 2017, PAI79170027.

Appendix A. Supporting information

Supplementary data associated with this article can be found in the online version at doi:10.1016/j.cattod.2021.06.027.

References

[1] M. Shokouhimehr, K. Hong, T.H. Lee, C.W. Moon, S.P. Hong, K. Zhang, J.M. Suh, K. S. Choi, R.S. Varma, H.W. Jang, Magnetically retrievable nanocomposite adorned with Pd nanocatalysts: efficient reduction of nitroaromatics in aqueous media, Green Chem. 20 (2018) 3809–3817.

[2] N. Daems, J. Wouters, C. Van Goethem, K. Baert, C. Poleunis, A. Delcorte, A. Hubin, I.F.J. Vankelecom, P.P. Pescarmona, Selective reduction of nitrobenzene to aniline over electrocatalysts based on nitrogen-doped carbons containing non-noble metals, Appl. Catal. B: Environ. 226 (2018) 509–522.

[3] S. Doherty, J.G. Knight, T. Backhouse, R.J. Summers, E. Abood, W. Simpson, W. Paget, R.A. Bourne, T.W. Chamberlain, R. Stones, K.R.J. Lovelock, J. M. Seymour, M.A. Isaacs, C. Hardacre, H. Daly, N.H. Rees, Highly selective and solvent-dependent reduction of nitrobenzene to N-phenylhydroxylamine, azoxybenzene, and aniline catalyzed by phosphino-modified polymer immobilized ionic liquid-stabilized AuNPs, ACS Catal. 9 (2019) 4777–4791.

[4] Y. Ma, Z. Lang, J. Du, L. Yan, Y. Wang, H. Tan, S.U. Khan, Y. Liu, Z. Kang, Y. Li, A switchable-selectivity multiple-interface Ni-WC hybrid catalyst for efficient nitroarene reduction, J. Catal. 377 (2019) 174–182.

[5] M. Cortes-Clerget, N.R. Lee, B.H. Lipshutz, Synthetic chemistry in water: applications to peptide synthesis and nitro-group reductions, Nat. Protoc. 14 (2019) 1108–1129.

[6] J.J. Song, Z.F. Huang, L. Pan, K. Li, X.W. Zhang, L. Wang, J.J. Zou, Review on selective hydrogenation of nitroarene by catalytic, photocatalytic and electrocatalytic reactions, Appl. Catal. B-Environ. 227 (2018) 386–408.

[7] C.K.P. Neeli, P. Puthiaraj, Y.-R. Lee, Y.-M. Chung, S.-H. Baeck, W.-S. Ahn, Transfer hydrogenation of nitrobenzene to aniline in water using Pd nanoparticles immobilized on amine-functionalized UiO-66, Catal. Today 303 (2018) 227–234.

[8] Sheldon, R.A. and van Bekkum, H., Catalytic Hydrogenation and Dehydrogenation, Fine Chemicals through Heterogeneous Catalysis, 2000, pp. 351-471.

[9] A. Grirrane, A. Corma, H. García, Gold-catalyzed synthesis of aromatic azo compounds from anilines and nitroaromatics, Science 322 (2008) 1661–1664.

[10] F.A. Westerhaus, R.V. Jagadeesh, G. Wienhöfer, M.-M. Pohl, J. Radnik, A.-E. Surkus, J. Rabeah, K. Junge, H. Junge, M. Nielsen, A. Brückner, M. Beller, Heterogenized cobalt oxide catalysts for nitroarene reduction by pyrolysis of molecularly defined complexes, Nat. Chem. 5 (2013) 537–543.

[11] H. Wei, X. Liu, A. Wang, L. Zhang, B. Qiao, X. Yang, Y. Huang, S. Miao, J. Liu, T. Zhang, FeOx-supported platinum single-atom and pseudo-single-atom catalysts for chemoselective hydrogenation of functionalized nitroarenes, Nat. Commun. 5 (2014) 5634.

[12] K. Junge, B. Wendt, N. Shaikh, M. Beller, Iron-catalyzed selective reduction of nitroarenes to anilines using organosilanes, Chem. Commun. 46 (2010) 1769–1771.

[13] S. Zhang, C.-R. Chang, Z.-Q. Huang, J. Li, Z. Wu, Y. Ma, Z. Zhang, Y. Wang, Y. Qu, High catalytic activity and chemoselectivity of sub-nanometric Pd clusters on porous nanorods of CeO_2 for hydrogenation of nitroarenes, J. Am. Chem. Soc. 138 (2016) 2629–2637.

[14] Z.-N. Hu, Y. Ai, L. Liu, Y. Chen, X. Song, J. Li, J. Yu, H. Tian, R. Guo, H.-b. Sun, J. Hu, Q. Liang, A predictable catalyst model for highly active and selective catalysis of hydrogenation of nitroarenes: comprehension of various precious metal nanoparticles, ChemistrySelect 4 (2019) 8960–8967.

[15] F. Cárdenas-Lizana, B. Bridier, C.C.K. Shin, J. Pérez-Ramírez, L. Kiwi-Minsker, Promotional effect of Ni in the selective gas-phase hydrogenation of chloronitrobenzene over Cu-based catalysts, ChemCatChem 4 (2012) 668–673.

[16] K. Currall, S.D. Jackson, Hydrogenation of 4-nitroacetophenone over Rh/silica, Appl. Catal. A: Gen. 484 (2014) 59–63.

[17] L. Liu, P. Concepción, A. Corma, Non-noble metal catalysts for hydrogenation: a facile method for preparing Co nanoparticles covered with thin layered carbon, J. Catal. 340 (2016) 1–9.

[18] K.-i Shimizu, Y. Miyamoto, A. Satsuma, Size- and support-dependent silver cluster catalysis for chemoselective hydrogenation of nitroaromatics, J. Catal. 270 (2010) 86–94.

[19] M. Tamura, N. Yuasa, Y. Nakagawa, K. Tomishige, Selective hydrogenation of nitroarenes to aminoarenes using a MoOx-modified Ru/SiO_2 catalyst under mild conditions, Chem. Commun. 53 (2017) 3377–3380.

[20] Y. Tan, X.Y. Liu, L. Zhang, A. Wang, L. Li, X. Pan, S. Miao, M. Haruta, H. Wei, H. Wang, F. Wang, X. Wang, T. Zhang, ZnAl-hydrotalcite-supported Au25 nanoclusters as precatalysts for chemoselective hydrogenation of 3-nitrostyrene, Angew. Chem. Int. Ed. 56 (2017) 2709–2713.

[21] S. Xu, D. Yu, S. Liao, T. Ye, H. Sheng, Nitrogen-doped carbon supported iron oxide as efficient catalysts for chemoselective hydrogenation of nitroarenes, RSC Adv. 6 (2016) 96431–96435.

[22] H.K. Kadam, S.G. Tilve, Copper(ii) bromide as a procatalyst for in situ preparation of active Cu nanoparticles for reduction of nitroarenes, RSC Adv. 2 (2012) 6057–6060.

[23] H. Yoshida, N. Igarashi, S.-i Fujita, J. Panpranot, M. Arai, Influence of crystallite size of TiO_2 supports on the activity of dispersed Pt catalysts in liquid-phase selective hydrogenation of 3-nitrostyrene, nitrobenzene, and styrene, Catal. Lett. 145 (2015) 606–611.

[24] Q. Chen, M. Wang, C. Zhang, K. Ren, Y. Xin, M. Zhao, E. Xing, Selectivity control on hydrogenation of substituted nitroarenes through end-on adsorption of reactants in zeolite-encapsulated platinum nanoparticles, Chem. – Asian J. 13 (2018) 2077–2084.

[25] J. Gu, Z. Zhang, P. Hu, L. Ding, N. Xue, L. Peng, X. Guo, M. Lin, W. Ding, Platinum nanoparticles encapsulated in MFI zeolite crystals by a two-step dry gel conversion method as a highly selective hydrogenation catalyst, ACS Catal. 5 (2015) 6893–6901.

[26] C. Wang, S. Mao, Z. Wang, Y. Chen, W. Yuan, Y. Ou, H. Zhang, Y. Gong, Y. Wang, B. Mei, Z. Jiang, Y. Wang, Insight into single-atom-induced unconventional size dependence over CeO_2-supported Pt catalysts, Chem 6 (2020) 752–765.

[27] P. Jing, T. Gan, H. Qi, B. Zheng, X. Chu, G. Yu, W. Yan, Y. Zou, W. Zhang, G. Liu, Synergism of Pt nanoparticles and iron oxide support for chemoselective hydrogenation of nitroarenes under mild conditions, Chin. J. Catal. 40 (2019) 214–222.

[28] T. Gao, W. Shi, Y. Zhang, L. Zhang, B. Zhang, Z.-W. Liu, Finely controlled platinum nanoparticles over ZnO nanorods for selective hydrogenation of 3-nitrostyrene to 3-vinylaniline, Chem. – Eur. J. 26 (2020) 8990–8996.

[29] Y. Sheng, X. Lin, X. Wang, X. Zou, C. Zhang, Highly dispersed Pt nanoparticles on N-doped ordered mesoporous carbon as effective catalysts for selective hydrogenation of nitroarenes, Catalysts 10 (2020) 374.

[30] W. Shi, B. Zhang, Y. Lin, Q. Wang, Q. Zhang, D.S. Su, Enhanced chemoselective hydrogenation through tuning the interaction between Pt nanoparticles and carbon supports: insights from identical location transmission electron microscopy and X-ray photoelectron spectroscopy, ACS Catal. 6 (2016) 7844–7854.

[31] J. Li, X. Li, Y. Ding, P. Wu, Pt nanoparticles entrapped in ordered mesoporous carbons: an efficient catalyst for the liquid-phase hydrogenation of nitrobenzene and its derivatives, Chin. J. Catal. 36 (2015) 1995–2003.

[32] J. Zhang, Y. Deng, X. Cai, Y. Chen, M. Peng, Z. Jia, Z. Jiang, P. Ren, S. Yao, J. Xie, D. Xiao, X. Wen, N. Wang, H. Liu, D. Ma, Tin-assisted fully exposed platinum clusters stabilized on defect-rich graphene for dehydrogenation reaction, ACS Catal. 9 (2019) 5998–6005.

[33] S.-M. Wu, X.-Y. Yang, C. Janiak, Confinement effects in zeolite-confined noble metals, Angew. Chem. Int. Ed. 58 (2019) 12340–12354.

[34] T. TrangNguyen, P. Serp, Confinement of metal nanoparticles in carbon nanotubes, ChemCatChem 5 (2013) 3595–3603.

[35] H. Wang, L. Wu, A. Jia, X. Li, Z. Shi, M. Duan, Y. Wang, Ni nanoparticles encapsulated in the channel of titanate nanotubes: efficient noble-metal-free catalysts for selective hydrogen generation from hydrous hydrazine, Chem. Eng. J. 332 (2018) 637–646.

[36] H. Liu, L. Zhang, N. Wang, D.S. Su, Palladium nanoparticles embedded in the inner surfaces of carbon nanotubes: synthesis, catalytic activity, and sinter resistance, Angew. Chem. Int. Ed. 53 (2014) 12634–12638.

[37] N. Goswami, B. Biswas, R. Naidu, K. Vasilev, Spatially localized synthesis of metal nanoclusters on clay nanotubes and their catalytic performance, ACS Sustain. Chem. Eng. 7 (2019) 18350–18358.

[38] M. Massaro, C.G. Colletti, G. Lazzara, S. Milioto, R. Noto, S. Riela, Halloysite nanotubes as support for metal-based catalysts, J. Mater. Chem. A 5 (2017) 13276–13293.

[39] X. Li, Y. Jiang, R. Zhou, Z. Hou, Acetalization of glycerol with acetone over appropriately-hydrophobic zirconium organophosphonates, Appl. Clay Sci. 189 (2020), 105555.

[40] A. Glotov, A. Stavitskaya, Y. Chudakov, E. Ivanov, W. Huang, V. Vinokurov, A. Zolotukhina, A. Maximov, E. Karakhanov, Y. Lvov, Mesoporous metal catalysts templated on clay nanotubes, Bull. Chem. Soc. Jpn. 92 (2019) 61–69.

[41] S. Saadat, G. Pandey, M. Tharmavaram, V. Braganza, D. Rawtani, Nano-interfacial decoration of Halloysite Nanotubes for the development of antimicrobial nanocomposites, Adv. Colloid Interface Sci. 275 (2020), 102063.

[42] V.A. Vinokurov, A.V. Stavitskaya, A.P. Glotov, A.A. Novikov, A.V. Zolotukhina, M. S. Kotelev, P.A. Gushchin, E.V. Ivanov, Y. Darrat, Y.M. Lvov, Nanoparticles formed onto/into halloysite clay tubules: architectural synthesis and applications, Chem. Rec. 18 (2018) 858–867.

[43] N. Danyliuk, J. Tomaszewska, T. Tatarchuk, Halloysite nanotubes and halloysite-based composites for environmental and biomedical applications, J. Mol. Liq. 309 (2020), 113077.

[44] J. Hamdi, A.A. Blanco, B. Diehl, J.B. Wiley, M.L. Trudell, Room-temperature aqueous suzuki–miyaura cross-coupling reactions catalyzed via a recyclable palladium@halloysite nanocomposite, Org. Lett. 21 (2019) 3471–3475.

[45] V. Vinokurov, A. Glotov, Y. Chudakov, A. Stavitskaya, E. Ivanov, P. Gushchin, A. Zolotukhina, A. Maximov, E. Karakhanov, Y. Lvov, Core/shell ruthenium–halloysite nanocatalysts for hydrogenation of phenol, Ind. Eng. Chem. Res. 56 (2017) 14043–14052.

[46] S. Noël, A. Madureira, B. Léger, A. Ponchel, S. Sadjadi, É. Monflier, Cyclodextrin-assisted catalytic hydrogenation of hydrophobic substrates with halloysite immobilized ruthenium NPs dispersed in aqueous phase, J. Indian Chem. Soc. 98 (2021), 100034.

[47] T. Yang, M. Du, M. Zhang, H. Zhu, P. Wang, M. Zou, Synthesis and immobilization of Pt nanoparticles on amino-functionalized halloysite nanotubes toward highly active catalysts, Nanomater. Nanotechnol. 5 (2015) 4.

[48] X. Gao, F. Tang, Z. Jin, Pt–Cu bimetallic nanoparticles loaded in the lumen of halloysite nanotubes, Langmuir 35 (2019) 14651–14658.

[49] S. Sadjadi, M. Akbari, B. Léger, E. Monflier, M.M. Heravi, Eggplant-derived biochar-halloysite nanocomposite as supports of Pd nanoparticles for the catalytic hydrogenation of nitroarenes in the presence of cyclodextrin, ACS Sustain. Chem. Eng. 7 (2019) 6720–6731.
[50] K. Shanmugaraj, T.M. Bustamante, C.H. Campos, C.C. Torres, Liquid phase hydrogenation of pharmaceutical interest nitroarenes over gold-supported alumina nanowires catalysts, Materials 13 (2020).
[51] T.M. Bustamante, C.H. Campos, M.A. Fraga, J.L.G. Fierro, G. Pecchi, Promotional effect of palladium in Co-SiO2 core@shell nanocatalysts for selective liquid phase hydrogenation of chloronitroarenes, J. Catal. 385 (2020) 224–237.
[52] D. González-Vera, T.M. Bustamante, J.N.D. de León, R. Dinamarca, R. Morales, P. A. Osorio-Vargas, C.C. Torres, C.H. Campos, Chemoselective nitroarene hydrogenation over Ni-Pd alloy supported on TiO_2 prepared from ilmenite-type $Pd_xNi_{1-x}TiO_3$, Mater. Today Commun. 24 (2020), 101091.
[53] T.M. Bustamante, R. Dinamarca, C.C. Torres, G. Pecchi, C.H. Campos, Pd-Co catalysts prepared from palladium-doped cobalt titanate precursors for chemoselective hydrogenation of halonitroarenes, Mol. Catal. 482 (2020), 110702.
[54] J.H. Shen, Y. Zhou, J.F. Huang, Y.H. Zhu, J.R. Zhu, X.L. Yang, W. Chen, Y.F. Yao, S. H. Qian, H. Jiang, C.Z. Li, In-situ SERS monitoring of reaction catalyzed by multifunctional Fe_3O_4@TiO_2@Ag-Au microspheres, Appl. Catal. B-Environ. 205 (2017) 11–18.
[55] Á. Álvarez, J. Yáñez, Screening of gunshot residue in skin using attenuated total reflection fourier transform infrared (ATR FT-IR) hyperspectral microscopy, Appl. Spectrosc. 74 (2020) 400–407.
[56] P. Yuan, P.D. Southon, Z.W. Liu, M.E.R. Green, J.M. Hook, S.J. Antill, C.J. Kepert, Functionalization of halloysite clay nanotubes by grafting with gamma-aminopropyltriethoxysilane, J. Phys. Chem. C 112 (2008) 15742–15751.
[57] K. Fidecka, J. Giacoboni, P. Picconi, R. Vago, E. Licandro, Quantification of amino groups on halloysite surfaces using the Fmoc-method, RSC Adv. 10 (2020) 13944–13948.
[58] S. Jia, M. Fan, Silanization of heat-treated halloysite nanotubes using γ-aminopropyltriethoxysilane, Appl. Clay Sci. 180 (2019), 105204.
[59] W.A. Spieker, J. Liu, J.T. Miller, A.J. Kropf, J.R. Regalbuto, An EXAFS study of the co-ordination chemistry of hydrogen hexachloroplatinate(IV): 1. Speciation in aqueous solution, Appl. Catal. A: Gen. 232 (2002) 219–235.
[60] E. Mäkilä, L.M. Bimbo, M. Kaasalainen, B. Herranz, A.J. Airaksinen, M. Heinonen, E. Kukk, J. Hirvonen, H.A. Santos, J. Salonen, Amine modification of thermally carbonized porous silicon with silane coupling chemistry, Langmuir 28 (2012) 14045–14054.
[61] F. Huang, Y. Deng, Y. Chen, X. Cai, M. Peng, Z. Jia, P. Ren, D. Xiao, X. Wen, N. Wang, H. Liu, D. Ma, Atomically dispersed Pd on nanodiamond/graphene hybrid for selective hydrogenation of acetylene, J. Am. Chem. Soc. 140 (2018) 13142–13146.
[62] Y.H. Ahmad, A.T. Mohamed, W.M.I. Hassan, A. Soliman, K.A. Mahmoud, A. S. Aljaber, S.Y. Al-Qaradawi, Bimetallic palladium-supported halloysite nanotubes for low temperature CO oxidation: experimental and DFT insights, Appl. Surf. Sci. 493 (2019) 70–80.
[63] A. Glotov, A. Vutolkina, A. Pimerzin, V. Nedolivko, G. Zasypalov, V. Stytsenko, E. Karakhanov, V. Vinokurov, Ruthenium catalysts templated on mesoporous MCM-41 type silica and natural clay nanotubes for hydrogenation of benzene to cyclohexane, Catalysts 10 (2020) 537.
[64] S.L. Bergman, J. Granestrand, Y. Tang, R.S. París, M. Nilsson, F.F. Tao, C. Tang, S. J. Pennycook, L.J. Pettersson, S.L. Bernasek, In-situ characterization by Near-Ambient Pressure XPS of the catalytically active phase of Pt/Al_2O_3 during NO and CO oxidation, Appl. Catal. B: Environ. 220 (2018) 506–511.
[65] B. Dong, Y. Li, X. Ning, H. Wang, H. Yu, F. Peng, Trace iron impurities deactivate palladium supported on nitrogen-doped carbon nanotubes for nitrobenzene hydrogenation, Appl. Catal. A: Gen. 545 (2017) 54–63.
[66] C.C. Torres, V.A. Jimenez, C.H. Campos, J.B. Alderete, R. Dinamarca, T. M. Bustamente, B. Pawelec, Gold catalysts supported on TiO_2-nanotubes for the selective hydrogenation of p-substituted nitrobenzenes, Mol. Catal. 447 (2018) 21–27.
[67] X.L. Yan, P. Duan, F.W. Zhang, H. Li, H.X. Zhang, M. Zhao, X.M. Zhang, B.S. Xu, S. J. Pennycook, J.J. Guo, Stable single-atom platinum catalyst trapped in carbon onion graphitic shells for improved chemoselective hydrogenation of nitroarenes, Carbon 143 (2019) 378–384.
[68] Y. Sheng, X.G. Wang, Z.K. Xing, X.B. Chen, X.J. Zou, X.G. Lu, Highly active and chemoselective reduction of halogenated nitroarenes catalyzed by ordered mesoporous carbon supported platinum nanoparticles, ACS Sustain. Chem. Eng. 7 (2019) 8908–8916.
[69] Z.Y. Sun, Y.F. Zhao, Y. Xie, R.T. Tao, H.Y. Zhang, C.L. Huang, Z.M. Liu, The solvent-free selective hydrogenation of nitrobenzene to aniline: an unexpected catalytic activity of ultrafine Pt nanoparticles deposited on carbon nanotubes, Green. Chem. 12 (2010) 1007–1011.
[70] R.F. Nie, J.H. Wang, L.N. Wang, Y. Qin, P. Chen, Z.Y. Hou, Platinum supported on reduced graphene oxide as a catalyst for hydrogenation of nitroarenes, Carbon 50 (2012) 586–596.
[71] Y.F. Zhao, H.Y. Zhang, C.L. Huang, S. Chen, Z.M. Liu, Pt/titania/reduced graphite oxide nanocomposite: an efficient catalyst for nitrobenzene hydrogenation, J. Colloid Interface Sci. 374 (2012) 83–88.
[72] G.Y. Fan, Y.H. Wang, C.Y. Wang, One-pot synthesis of aluminum oxyhydroxide matrix-entrapped Pt nanoparticles as an excellent catalyst for the hydrogenation of nitrobenzene, RSC Adv. 4 (2014) 10997–11002.
[73] F. Zhang, C. Zhao, S. Chen, H. Li, H. Yang, X.-M. Zhang, In situ mosaic strategy generated Co-based N-doped mesoporous carbon for highly selective hydrogenation of nitroaromatics, J. Catal. 348 (2017) 212–222.
[74] M. Turáková, T. Salmi, K. Eränen, J. Wärnå, D.Y. Murzin, M. Králik, Liquid phase hydrogenation of nitrobenzene, Appl. Catal. A: Gen. 499 (2015) 66–76.
[75] G.D. Yadav, R.K. Mewada, Novelties of azobenzene synthesis via selective hydrogenation of nitrobenzene over nano-fibrous Ag-OMS-2 – Mechanism and kinetics, Chem. Eng. J. 221 (2013) 500–511.
[76] J. Yao, Z. He, J. Chen, W. Sun, H. Fang, W. Xu, Design, synthesis and biological activities of sorafenib derivatives as antitumor agents, Bioorg. Med. Chem. Lett. 22 (2012) 6549–6553.
[77] A. Mahajan, P. Gupta, Halloysite nanotubes based heterogeneous solid acid catalysts, New J. Chem. 44 (2020) 12897–12908.
[78] H. Jin, J. Zhou, T. Pu, A. Zhang, X. Gao, K. Tao, T. Hou, Synthesis of novel fenfuram-diarylether hybrids as potent succinate dehydrogenase inhibitors, Bioorg. Chem. 73 (2017) 76–82.